#1174

Spatially Distributed Sensible Heat Flux over a Semiarid Watershed. Part I: Use of Radiometric Surface Temperatures and a Spatially Uniform Resistance

K. S. HUMES*

Department of Geography, University of Oklahoma, Norman, Oklahoma

W. P. KUSTAS

USDA/ARS Hydrology Laboratory, Natural Resources Institute, Beltsville, Maryland

D. C. GOODRICH

USDA/ARS Southwest Watershed Research Center, Tucson, Arizona

(Manuscript received 5 July 1995, in final form 10 June 1996)

ABSTRACT

Spatially distributed radiometric surface temperatures over a semiarid watershed were computed using remotely sensed data acquired with an aircraft-based multispectral scanner during the Monsoon '90 Large Scale Field Experiment. The multispectral scanner data provide watershed coverage of surface temperature at a resolution of 6.3 m and nearly daily temporal resolution. At high spatial resolution, the surface temperature values appear to be correlated strongly with surface aspect; at more coarse spatial resolution, the surface temperatures variations across the watershed appear to be correlated with background soil moisture variations caused by highly localized precipitation events. The surface temperature data were aggregated to 400-m spatial resolution for the purpose of computing spatially distributed sensible heat fluxes over the watershed. The practicality of using a spatially uniform transfer coefficient was evaluated by examining the variability of surface and meteorological factors across the watershed at the times of the aircraft overpasses. Maps of sensible heat flux over the area were computed for three aircraft overpass dates and compared to localized patterns of recent precipitation in the basin. Maps of instantaneous sensible heat flux tracked well with the spatial patterns of variable surface soil moisture that arose from the localized precipitation events.

1. Introduction

Remotely sensed data are the only tools that have the potential to provide spatially distributed information relating to land surface parameters and state variables on a regular basis and over a range of spatial scales. This information is potentially very useful in hydrology and meteorology for quantifying the spatially distributed parameters and variables that control the interaction of land surface and atmospheric processes. In particular, surface temperature fields and spatially distributed surface fluxes estimated from remotely sensed data could be very useful as boundary conditions and/or validation fields for atmospheric models.

While not all attempts to utilize radiative surface temperature for estimating sensible heat flux have been successful (Hall et al. 1992), radiative surface temperatures have been shown by some researchers to be useful for the estimation of surface fluxes for both agricultural surfaces (Reginato et al. 1985; Jackson 1985) and sparsely vegetated surfaces (Kustas et al. 1989; Moran et al. 1994; Kustas et al. 1994a; Stewart et al. 1994). Some of these efforts have included the estimation of spatially distributed sensible heat flux (Moran et al. 1990; Holwill and Stewart 1992). Verification of model output over large areas is not straightforward because few field studies contain an adequate number of ground flux measurements to be used for verification of remotely sensed estimates over the different land surface types often involved in large-scale field experiments. Eventually, the continuous simulation of spatially distributed water and energy fluxes will require the merging of remotely sensed data with more complicated physically based models, thereby providing as many constraints as possible on the problem (e.g., Carlson et al. 1981; Taconet et al. 1986; Sellers et al. 1986). How-

* The work described in this paper was carried out while the author was at the USDA/ARS Hydrology Laboratory, Beltsville, Maryland.

Corresponding author address: Dr. Karen S. Humes, Department of Geography, SEC Room 684, University of Oklahoma, Norman, OK 73019-0628.
E-mail: khumes@ou.edu

© 1997 American Meteorological Society

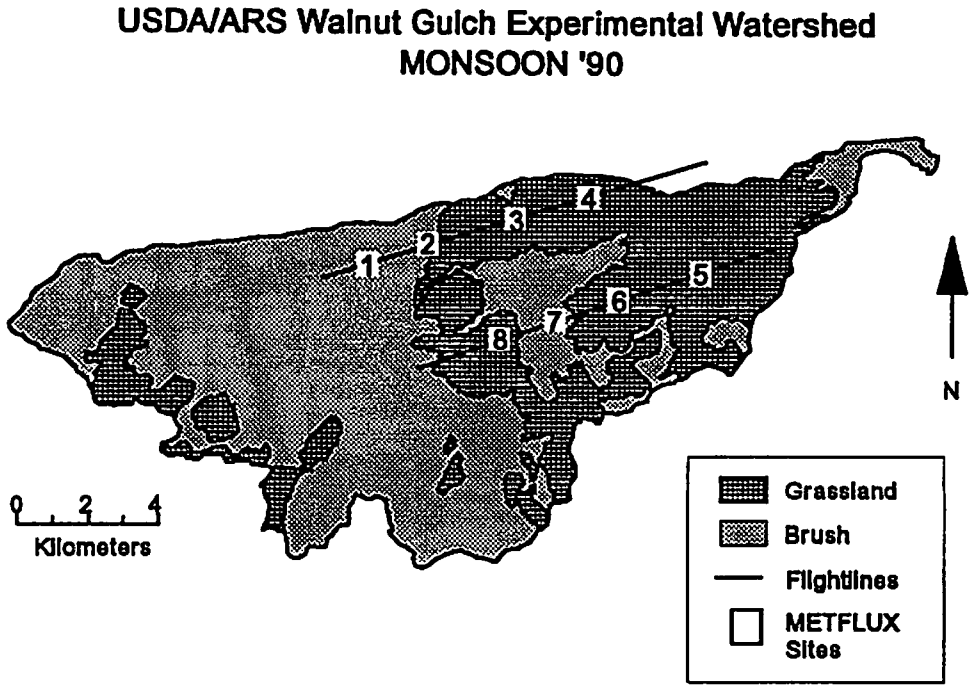

FIG. 1. A diagram of the USDA/ARS Walnut Gulch Experimental Watershed, site of the Monsoon '90 field experiment. The straight lines represent the transect lines flown by the C-130 aircraft from which the NS001 multispectral scanner data were acquired.

ever, future improvements in these types of models will require a reduction in the number of parameters and variables for which a priori knowledge is required, especially those quantities for which spatially distributed information is rarely, if ever, available.

The main thrust of this paper is not to demonstrate a generalized ideal method for estimating surface energy balance components with remotely sensed data, but rather to utilize a very unique set of measurements in a special field campaign to generate spatially distributed sensible heat flux estimates for a specific site with as little error as possible. These maps are then compared to the spatial patterns of recent precipitation events over the watershed to visualize the impact of highly localized precipitation events on surface energy balance across the watershed. Thus, a relatively simple procedure was used for estimating spatially distributed sensible heat flux from aircraft-based surface temperature data acquired over a semiarid watershed. The remotely sensed surface temperatures were measured from an aircraft platform that provided high spatial and temporal resolution data. The surface temperature data were acquired during midmorning periods just before and after several highly localized precipitation events in the basin. The variations in surface and meteorological factors that would be expected to affect the heat transfer coefficient across the watershed were evaluated. A spatially uniform transfer coefficient, computed with data from eight stations across the study site, was used to generate preliminary maps of sensible heat flux over the watershed. This relatively simple and straightforward method was chosen for this paper instead of more complicated methods that would require a priori knowledge of surface characteristics not known for other portions of the watershed (e.g., roughness lengths for heat and momentum) because it served to minimize the errors in the overall spatial patterns of sensible heat flux computed for the watershed. In a companion article (Kustas and Humes 1997), an algorithm is evaluated that utilizes additional ground-based information at the eight ground stations to test the effects of using spatially variable heat transfer coefficients at those stations.

2. Experiment and data

The data used in this analysis were collected during the Monsoon '90 field experiment (Kustas et al. 1991) conducted in the United States Department of Agriculture/Agricultural Research Service (USDA/ARS) Walnut Gulch Experimental Watershed (31.5°N, 110°W) maintained by the Southwest Watershed Research Center in Tucson, Arizona. The primary campaign of the Monsoon '90 experiment was conducted during a two-week period in the summer rainy season, a time at which the vegetation was very active. There is a transition in dominant vegetation types and density across the watershed. The eastern upland portions of the watershed are classified as desert grasslands; the west and west-central portions of the watershed are classified as a desert steppe-shrub community (see Fig. 1).

During the experiment, ground-, aircraft-, and satellite-based remotely sensed data were acquired at various spatial scales (Kustas and Goodrich 1994). The data used in this analysis were acquired with the NS001 sensor mounted in a National Aeronautics and Space Administration C-130 aircraft. On a number of days during the experiment, the aircraft flew along the transect lines shown in Fig. 1. The NS001 instrument has eight bands, seven of which nominally correspond to the seven bands on the Landsat Thematic Mapper instrument. The data used in this analysis were from the thermal band of the sensor (bandpass 10.9–12.3 μm). The instrument has the capability to scan across the flight track at angles of $\pm 50°$. Data used in this analysis were limited to scan angles of $\pm 20°$. The spatial resolution of the instrument is dependent on the altitude of the aircraft. The data used in this analysis were acquired at approximately 2400 m above the ground surface, corresponding to a pixel size of approximately 6 m $\times$ 6 m. Data from three days during the experiment, days of year (DOYs) 213, 216, and 221, were selected for this analysis. These days corresponded to periods just before and after localized precipitation events over the watershed, so these days represent dry, wet, and drying conditions over the watershed.

Ground-based measurements of surface temperature were made simultaneously with aircraft overpasses using instruments with similar bandpasses. The ground-based measurements were made with a backpack-type apparatus that allowed the acquisition of data over a large ground target area in a relatively short amount of time (Moran et al. 1994). These measurements were used to validate the calibration and atmospheric correction of surface temperature data from the NS001 instrument (Humes et al. 1997).

Ground-based measurements of surface energy fluxes and meteorological data were made at each of the eight METFLUX (meteorological and energy flux) stations shown in Fig. 1. Sensible heat flux was estimated at these stations with a temperature variance technique. The estimated accuracy of these measurements is approximately 20%. Instruments measuring temperature and wind speed were located at a nominal height of 4 m, and data averages over 20 min were recorded. A full description of the ground-based surface flux instrumentation and the flux computation technique is provided in Kustas et al. (1991) and Kustas et al. (1994b).

3. Results

a. Comparison of ground- and aircraft-based temperatures

Humes et al. (1997) evaluated the overall quality of radiometric temperatures derived from the NS001 multispectral scanner data acquired during the Monsoon '90 experiment by correcting for atmospheric effects and comparing the resulting temperature with simultaneously acquired ground-based remote sensing measurements over two large target areas. In comparing ground- and aircraft-based measurements, it is not possible to clearly separate the effects of uncertainties in airborne instrument calibration from the effects of the intervening atmosphere (Wukelic et al. 1989). One can, however, obtain an overall level of confidence in the data by comparing datasets from a number of different aircraft altitudes and a number of different days with varying atmospheric characteristics. The dominant atmospheric effects in the thermal portion of the spectrum are caused by the absorption and emission of energy by atmospheric gases, particularly water vapor.

To summarize the results described in Humes et al. (1997), areas corresponding to the large target areas measured with ground-based sensors were extracted from the NS001 images, corrected for the effects of the atmosphere by using a radiative transfer model, and compared to the ground measurements. The radiative transfer code used for the analysis was LOWTRAN version 7 (Kniezys et al. 1988), with input of coincident on-site radiosonde profiles of atmospheric temperature and water vapor concentration. The radiosonde launches occurred within an hour of the C-130 overpasses (Hipps et al. 1994). It was found that for images acquired at an aircraft altitude of approximately 2400 m above ground level (AGL), the use of these coincident on-site atmospheric profiles as input to LOWTRAN 7 provided better agreement between aircraft- and ground-based surface temperatures than aircraft temperatures corrected with the use of standard atmospheric models available within LOWTRAN 7 (Humes et al. 1997). For aircraft data acquired at 2400 m AGL, the magnitude of the temperature correction varied a bit from day to day but was on the order of 3°–4°C.

A summary of the comparison of radiometric temperatures measured over two large target areas on each of 3 different days for aircraft overpasses at 2400 m AGL is shown in Fig. 2. One large target area was located in the shrub-dominated portion of the watershed, and one ground target area was located in the grass-dominated portion of the watershed. These target areas were approximately 0.3 and 0.5 km^2 for the shrub and grassland targets, respectively. The grass- and shrub-dominated target areas were located in different images on each day; the results shown in Fig. 2 thus represent the analysis of extracts from six different NS001 images. The results shown in Fig. 2 suggest that the aircraft-based radiometric temperatures generally agree with the ground-based temperature measurements to within about 1°–2°C and were systematically less than the ground-based measurements on all 3 days. The root-mean-square difference for all six cases is approximately 1.2°C.

b. Spatially distributed surface temperatures

The atmospheric corrections computed with LOWTRAN 7 for each image analyzed above were applied on a pixel-by-pixel basis to each of the entire images.

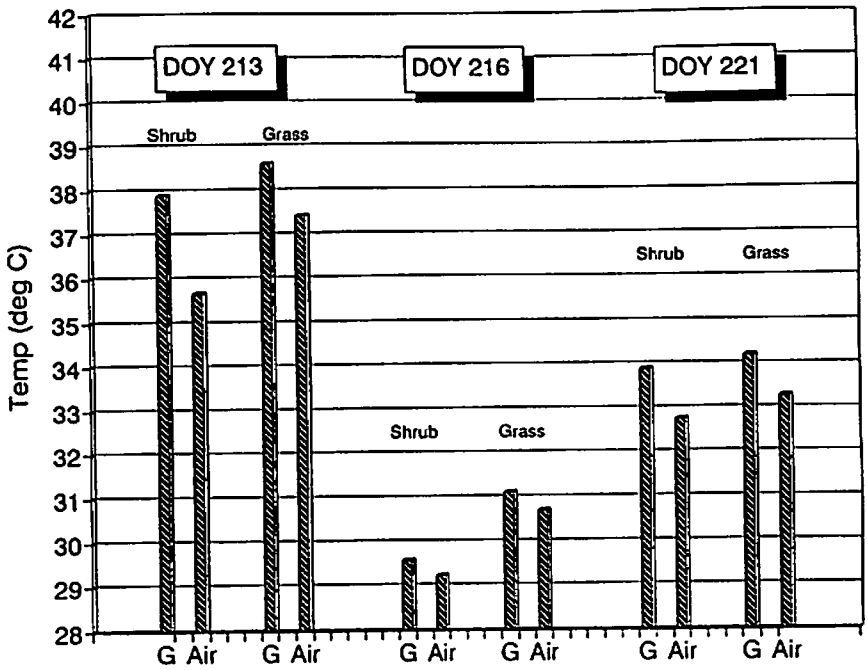

FIG. 2. Comparison of ground-based surface temperature measurements. The data bars labeled "G" correspond to radiometric temperatures measured with ground-based instruments mounted on a backpack-type apparatus. The data bars labeled "air" represent the radiometric temperatures derived from the NS001 data after correction for atmospheric effects, as computed by using the on-site radiosonde data as input into LOWTRAN 7. Results are shown for each of two large ground target areas on three different days.

Adjustments were made to the atmospheric corrections based on the scan angle across the image. Although the instrument is capable of scanning at ±50° perpendicular to the flight track, only data that were ±20° from nadir were used in this analysis, in order to minimize the effects of off-nadir view angles. On each day, it took approximately 15 min for the aircraft to fly the two flight lines required to provide coverage of most of the watershed. The two flight lines were superimposed together to provide coverage of most of the watershed. Because the pixel values in each image represent a quantitative estimate of the surface temperature, there was no interpolation done to improve the visual continuity of the two flight lines. The resulting discontinuities in the image are due to real physical effects, which are described below.

The full 6-m resolution atmospherically corrected, spatially distributed surface temperature data for DOYs 213, 216, and 221 is shown in Fig. 3. In the image for DOY 213, the isolated areas of low temperatures correspond to isolated cumulus clouds and cloud shadows present when the image was acquired. The image for DOY 213, and to a lesser degree the images for the other two days, shows discontinuities in surface temperatures between the two flight lines. These discontinuities are due to real physical effects, so no attempt was made to alter them. The northerly flight line was flown first, from west to east, and the southerly flight line was flown from east to west, resulting in a time difference of approximately 15 min for the acquisition of the westernmost portions of the north and south flight lines. Thus, the discontinuities are due to the time difference in the time data acquisition, together with the fact that in a semiarid environment such as this, surface heating is extremely rapid in the midmorning hours. The discontinuity is especially evident on DOY 213 because the surface soils were driest on that day and are especially evident in the western portion of the watershed because that is where the maximum time difference in data acquisition occurred. In all three images, the town of Tombstone, Arizona, can be seen in the southwestern corner of the area shown. The developed area shows both very hot pixels corresponding to buildings and roads, and very cool pixels corresponding to watered lawns.

At this high resolution, it appears that on a given day there is a high degree of correlation between surface temperature and aspect (e.g., northwest-facing versus southeast-facing slopes). Hipps et al. (1995) have undertaken an analysis of the length scales of variability in the surface temperature data, including a quantitative evaluation of the correlation between surface aspect and surface temperature. This correlation most likely arises because the soil surface heating is the dominant factor determining surface temperature for this sparsely vegetated landscape. Throughout all three images, the areas along the drainage patterns also appear relatively cool. This is most likely due both to shading of the surfaces

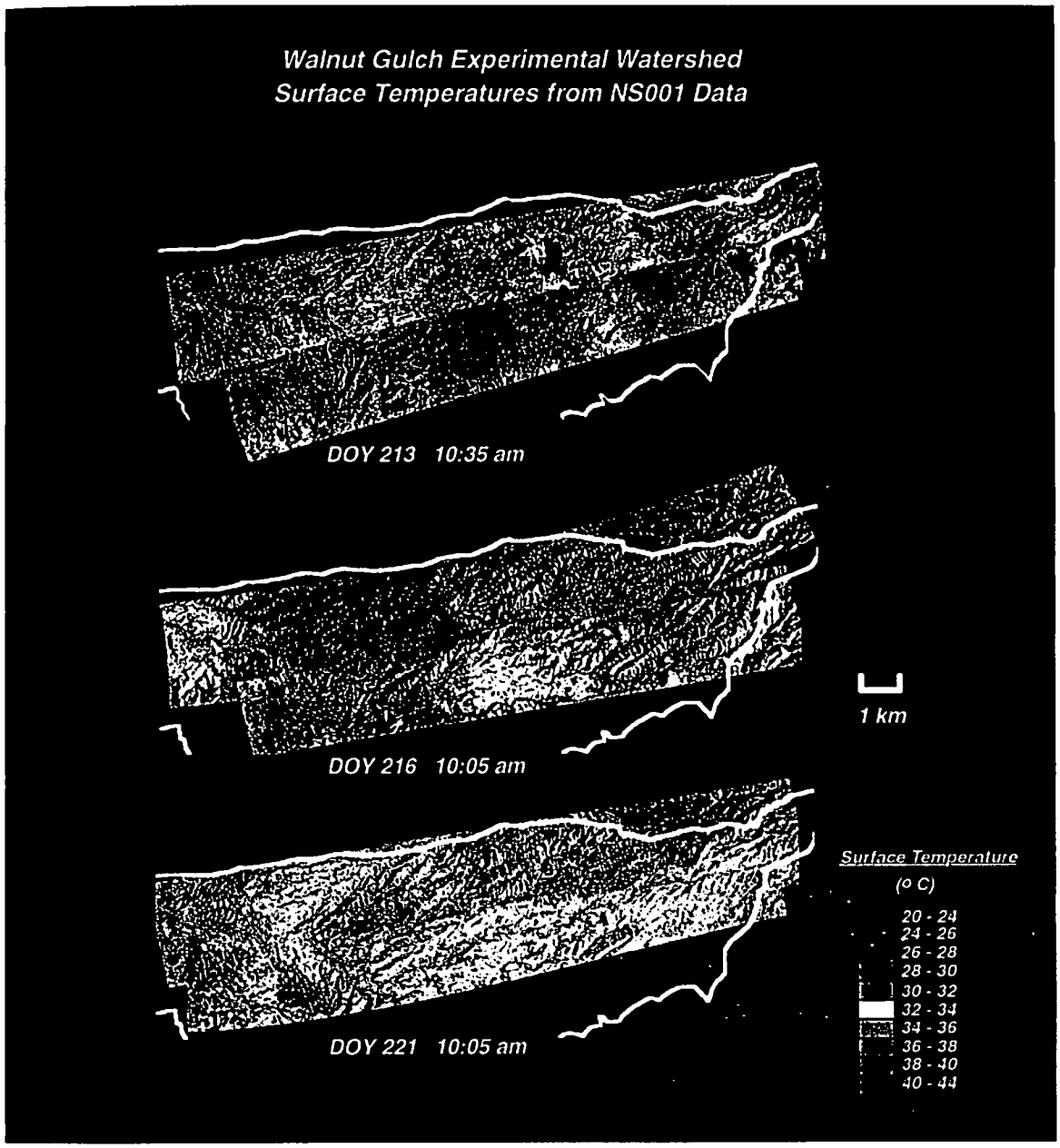

FIG. 3. Spatially distributed radiometric surface temperature values derived by applying atmospheric corrections to NS001 thermal band data over the entire watershed. The white lines represent the watershed boundaries. Temperatures are shown for DOYs 213, 216, and 221. The isolated dark spots on the image for DOY 213 correspond to clouds and cloud shadows present in the image during the aircraft overpass.

and to the presence of more dense channel-side vegetation along the desert washes.

To better evaluate the overall trends in surface temperature across the watershed and between days, it is useful to look at the spatially distributed patterns of soil moisture across the watershed on these days. The fractional vegetation cover over the watershed is on the order of 25%–55% (Weltz et al. 1994), so the composite surface temperature is largely determined by the surface soil temperature, which is strongly influenced by the surface soil moisture status. Humes et al. (1994) showed that during the rainy season portion of the experiment, the vegetation temperatures stayed within about 2°C of air temperature throughout the diurnal cycle, while the surface soil temperature warmed through the day in proportion to the surface soil moisture. Thus, for images acquired in the late morning period, areas with cooler surface temperatures would be expected to correspond to areas with moister surface soil conditions.

Passive microwave measurements in the L-band por-

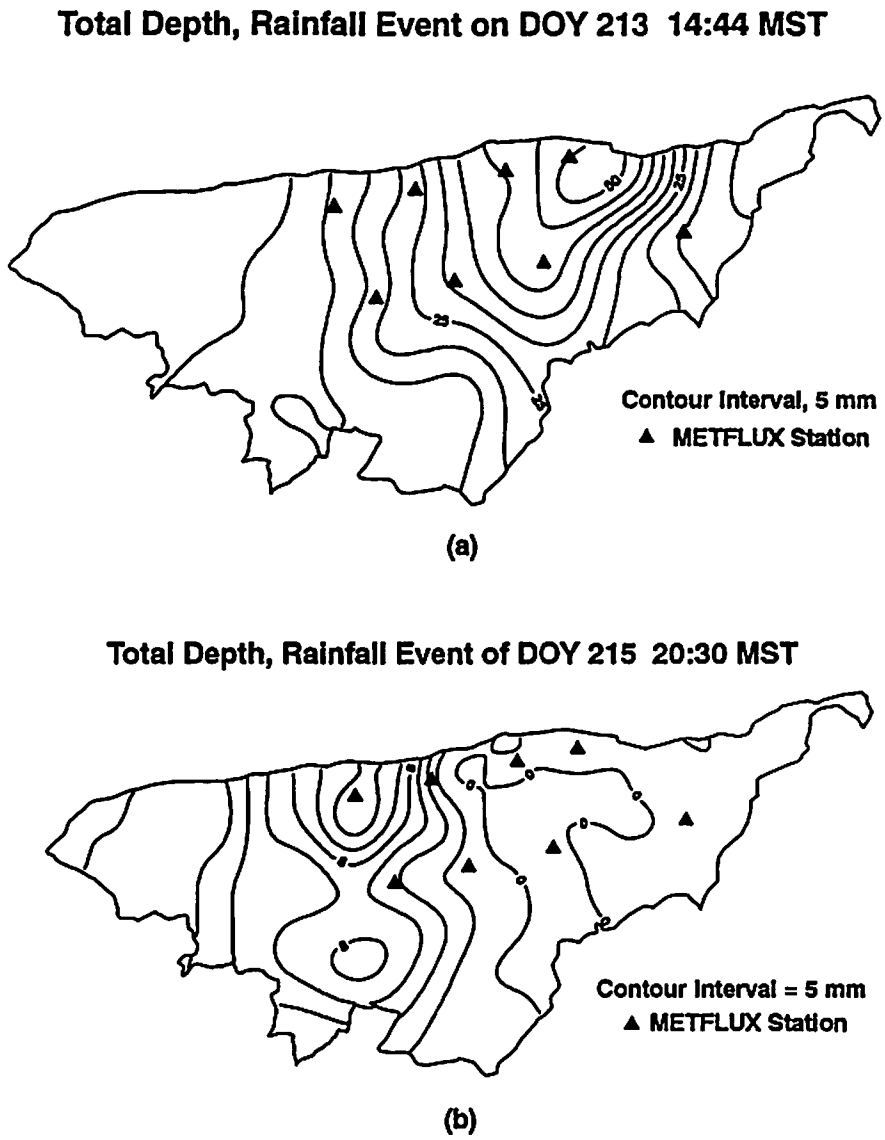

FIG. 4. Contours for the two most significant precipitation events occurring between the acquisition of the surface temperature images on DOY 213 and DOY 215.

tions of the spectrum were acquired nearly simultaneously by other airborne instruments used in the Monsoon '90 experiment (Kustas et al. 1991). These measurements have been demonstrated to be very strongly related to near-surface soil moisture (Schmugge et al. 1994). Over the Monsoon '90 experimental period, the passive microwave brightness temperatures had spatial patterns similar to those of the surface temperature images (Kustas et al. 1991). However, since passive microwave measurements are not routinely available for most areas, it is also useful to compare the surface temperature images to the spatial patterns of localized precipitation that occurred over the watershed just before and between the acquisition of the temperature images.

Before the main experimental period began on DOY 209, there had not been any significant precipitation events over the watershed for more than a week. The surface temperature image shown in Fig. 3 for DOY 213, which was acquired at approximately 1035 MST, shows fairly high surface temperatures, indicative of very dry surface soils across the watershed. Approximately 4 h after the temperature image for DOY 213 was acquired (i.e., at about 1444 MST), a relatively intense precipitation event occurred, which was centered over the northeastern portion of the watershed. Isohyets for this event, which were derived from the measurements acquired at 85 recording rain gauges, are shown in Fig. 4a. Several small and isolated events occurred during the midday hours on DOY 214 and DOY 215, which together contributed slightly more precipitation to both the northeastern edge of the watershed and the southwestern edge of the area shown in the images. Both

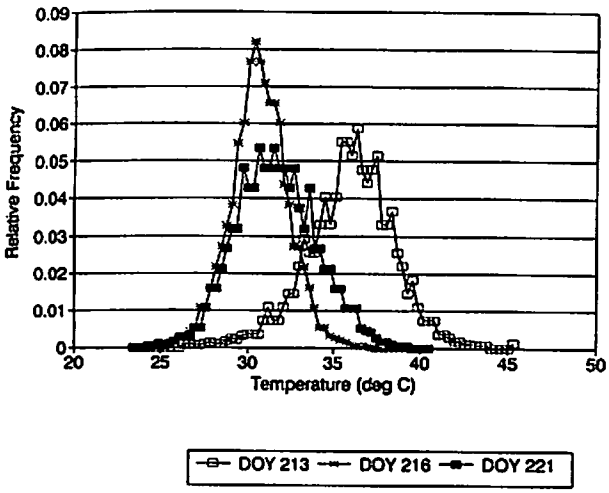

FIG. 5. Distribution of surface temperature values over the watershed on DOYs 213, 216, and 221. The data shown are derived from atmospherically corrected NS001 data over most of the watershed area.

of those days were mostly overcast, so only moderate drying occurred. The last precipitation event to occur before the next image was acquired was a relatively small event that occurred at approximately 2030 on DOY 215 (shown in Fig. 4b).

The next surface temperature image (1005 on DOY 216) was acquired approximately 10 h after this last event. The lower surface temperatures shown in the northwestern portion of the image correspond to the area that received the most (albeit very light) precipitation in the late-night DOY 215 event. Between the acquisition of the images on DOY 216 and DOY 221, there were two extremely small events (less than 3 mm), which were relatively uniformly distributed across the watershed. The image for DOY 221, since it was not preceded by any events just hours before acquisition, shows the effects of the longer-term drying from the more intense event on the afternoon of DOY 213.

In order to provide an overview of the variability in surface temperature on the different days, the distribution of surface temperatures for the three days is shown in Fig. 5. The mean temperature is highest (35.7°C) for DOY 213, due to the drier surface conditions and the slightly later time of day at which it was acquired. The standard deviation of surface temperature for DOY 213 was 3.0°C. On DOY 216, when most of the watershed was fairly moist, both the mean temperature (30.7°C) and the standard deviation (1.9°C) were smaller. By DOY 221, as the surface soils across the watershed were farther along in the drydown process and the uneven distribution of moisture resulted in more variability in surface soil moisture, the mean temperature (32.3°C) and the standard deviation (2.4°C) increased again. It is interesting to note that standard deviation in surface temperature for this period on each of the three days is substantially larger than the standard deviation in near-surface air temperature for those same periods (shown in Table 1 to be approximately 0.7°C).

TABLE 1. Mean and standard deviation of near-surface meteorological variables measured at eight METFLUX stations (4 m above the ground surface) during the averaging period closest to aircraft overpass times.

	T_{air} (°C)		Wind speed (m s^{-1})	
DOY	Mean	Standard deviation	Mean	Standard deviation
213	24.5	0.74	4.5	0.55
216	25.6	0.71	2.0	0.63
221	25.1	0.63	5.7	0.80

c. *Spatially distributed sensible heat flux*

The approach adopted here is to begin with the simplest expression for the relationship between surface temperature and sensible heat flux, the bulk transfer relationship. The suitability of the bulk transfer relationship for sensible heat flux, using radiometric surface temperature over sparsely vegetated surfaces, is a complex issue that will not be addressed here. Successful application of this type of relationship over semiarid surfaces is discussed in detail by Kustas et al. (1989), Moran et al. (1994), Kustas et al. (1994b), and Stewart et al. (1994). The bulk transfer relationship is given by the expression

$$H = \frac{\rho C_p (T_s - T_{air})}{r_{ah}}, \qquad (1)$$

where H (W m^{-2}) is the sensible heat flux for a given pixel, ρC_p is the volumetric heat capacity, T_s (K) is the radiometric surface temperature for a given pixel, and r_{ah} is the resistance to sensible heat transfer.

For all calculations described below using radiometric surface temperature, the 6.3-m pixels in the vicinity of the METFLUX stations were aggregated to 400-m pixels in order to be consistent with the approximate ground source area for the ground-based flux measurements acquired at a height of 4 m above the surface. In the companion paper (Kustas and Humes 1997), the relative contributions of ground source areas to the total flux measured at 4 m is discussed in more detail. For each overpass time on each day, the average wind direction measured at the eight ground flux stations was taken into consideration in selecting the area upwind of the flux stations to be used in the extraction of surface temperature in the vicinity of the flux stations.

Certainly, almost all parameters and variables that appear in a bulk transfer expression for sensible heat flux (e.g., near-surface air temperature, wind speed, and aerodynamic roughness parameters for momentum, which influence the transfer coefficient) do vary over a basin; however, these variables are typically only available from point-based measurements at a few locations in a basin. The approach adopted here is to begin with

TABLE 2. Values of surface–air temperature differences ($T_s - T_{air}$), in degrees Celsius, from ground measurements of T_{air} and values of T_s extracted from the surface temperature images in the vicinity of the METFLUX station, plus values of r_{ah} (s m^{-1}) computed using Eq. (1) with sensible heat flux measured at the ground-based METFLUX station and these values of $T_s - T_{air}$.

DOY	Site	Time (MST)	$T_s - T_{air}$	$r_{ah,calc}$
213	1	1030	10.0	41.8
	2	1030	11.5	54.0
	3	1030	11.3	58.3
	4	1030	12.5	53.3
	5	1030	13.6	61.2
	6	1030	12.3	59.9
	7	1030	13.8	66.3
	8	1030	13.8	67.1
				57.7 (Mean)
216	1	1010	3.4	38.2
	2	1010	4.4	48.7
	3	1010	5.1	74.6
	4	1010	5.8	48.6
	5	1010	5.9	47.7
	6	1010	5.6	43.4
	7	1010	5.6	71.9
	8	1010	7.0	88.2
				57.7 (Mean)
221	1	1010	8.3	52.3
	2	1010	6.5	49.0
	3	1010	5.4	37.3
	4	1010	6.9	49.0
	5	1010	8.8	56.5
	6	1010	7.7	61.2
	7	1010	10.0	66.8
	8	1010	8.4	43.3
				51.9 (Mean)

the simplest case of assuming all variables in the bulk transfer relationship to be constant over the watershed, except that quantity that can currently be derived from remotely sensed data, the radiometric surface temperature. The degree to which this assumption may cause errors in the estimation of sensible heat flux can be evaluated by examining the variability of the near-surface meteorological factors and surface factors that go into the bulk transfer expression.

1) EVALUATION OF VARIABILITY IN NEAR-SURFACE METEOROLOGICAL VARIABLES

Twenty-minute averages of near-surface temperature and wind speed (measured at 4-m screen height) were recorded at each of the eight METFLUX stations. For DOYs 216 and 221, the 20-min time period centered closest in time to the aircraft overpass time was used for this analysis. For DOY 213, there was significant temporal variation observed in the 20-min data, which was most likely due to intermittent cloudiness and changing meteorological conditions. For this day, an average of the three 20-min periods around the overpass time was used. The 20-min (DOYs 216 and 221) or hourly (DOY 213) average values for all meteorological

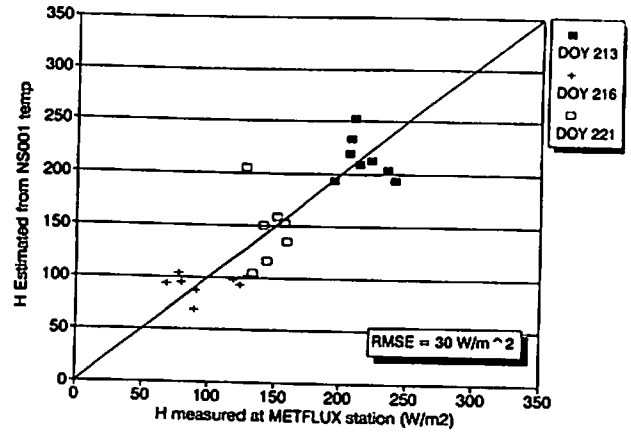

FIG. 6. Sensible heat fluxes estimated from NS001 radiometric surface temperature extracts over eight METFLUX stations on each of three days versus the sensible heat flux from ground-based flux measurements at each of the stations. Computations were made with a spatially uniform average value for r_{ah} over the basin.

variables for each METFLUX station are shown in Table 2 of Kustas and Humes (1997).

The mean and standard deviation of the air temperature T_{air} and wind speed for the eight METFLUX stations are shown in Table 1. The standard deviation in T_{air} for these time periods on the 3 days is roughly 0.6°–0.7°C. The standard deviation in wind speed among the eight stations varied from approximately 0.55 to 0.80 m s^{-1}. These variations are small enough that model attempts by Kustas and Humes (1997) to interpolate and/or extrapolate air temperatures and wind speeds from the METFLUX stations to other portions of the watershed resulted in uncertainties of roughly the same magnitude as these variations.

2) EVALUATION OF VARIABILITY IN TRANSFER COEFFICIENT

As a first step in evaluating the variability of the aerodynamic resistance across the watershed, the transfer coefficient was computed for each METFLUX site for each overpass by inverting Eq. (1) and using the measured values of H, T_{air} (from the ground-based flux stations), and T_s (from the remotely sensed images). The values of $T_s - T_{air}$ used for these calculations and the individual calculated values of aerodynamic resistance ($r_{ah,calc}$) are shown in Table 2.

For the individual days, the approximate range in values of r_{ah} were as follows: DOY 213 (42–67 s m^{-1}), DOY 216 (38–88 s m^{-1}), and DOY 221 (37–66 s m^{-1}). The day with the largest range in the value of r_{ah}, DOY 216, had H values ranging from 70 to 130 W m^{-2}, but small values of $T_s - T_{air}$. Thus, the uncertainties in the magnitude of r_{ah} for this day have a somewhat smaller impact on the uncertainty in H than would uncertainties in r_{ah} of the same magnitude for days with larger values of $T_s - T_{air}$.

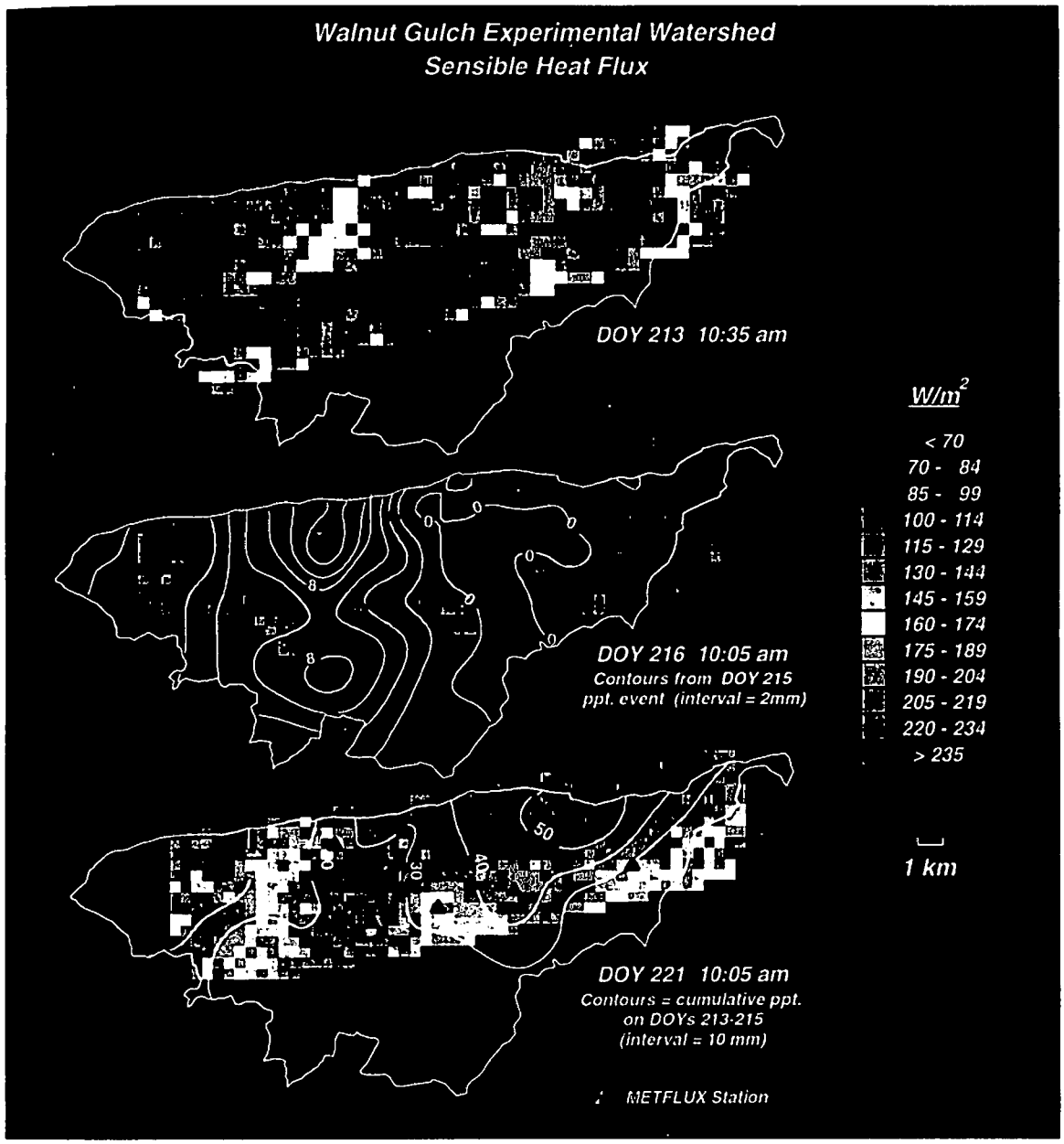

FIG. 7. Spatially distributed sensible heat flux values over the watershed for the three days of the aircraft overpasses. The fluxes were computed by aggregating the above surface temperature images to 400-m resolution and using the spatially uniform values of resistance for each day given in Table 2. Relevant precipitation contours are overlain for DOY 216 and DOY 221. For DOY 216, the precipitation contours are overlain for the event that occurred just 10 h before the image data were acquired. For DOY 221, the contours correspond to the cumulative precipitation for all significant events in the experimental period up to the acquisition of the image.

The differences in r_{ah} values among the stations could be expected to be related to many physical factors, including 1) variations in the values for the roughness length for momentum (z_{om}) between sites (particularly the shrub-dominated versus grass-dominated sites), 2) variations in the wind speed between sites, and 3) variations in the magnitude of $T_s - T_{air}$ values between sites. In considering the effect of factor 1, the values of z_{om} estimated at the eight METFLUX sites are given in Table 1 of Kustas and Humes (1997) and range from approximately 0.01 m for the site dominated by sparse grass to 0.10 m for a site dominated by tall desert shrubs. These differences are significant but not as large as those that would be encountered over areas of, say, mixed agricultural and wooded areas. In considering the second factor, the differences in r_{ah} arising from wind speed are likely to be fairly small given the intersite variability in wind speed shown in Table 1.

The contribution of the third factor to the variability in r_{ah} is more complicated to assess. One way in which the value of $T_s - T_{air}$ influences r_{ah} is through stability corrections, but this impact is likely to be very small. A more substantial effect is due to the relationship between $T_s - T_{air}$ and r_{ah} changing significantly over sparsely vegetated surfaces, even under similar environmental conditions, which inevitably requires adjustments to the roughness length for heat z_{oh}, expressed as $\ln(z_{om}/z_{oh})$ (Kustas and Humes 1997). A full discussion of this topic is outside the scope of this paper, but any approach to flux estimation with a single radiometric temperature over a sparse canopy requires consideration of the fact that there are actually multiple sources of sensible heat flux. Therefore, a single-source expression is inherently an oversimplified attempt to quantify the heat transfer with one radiometric temperature. Over a sparsely vegetated surface, with components (e.g., soil and vegetation) that are at extremely different temperatures, the components contribute to the composite radiometric temperature in proportion to the fraction of sensor viewing area they occupy. However, the components contribute to the heat flux in proportion to the temperature difference between the component and the atmosphere, and the degree to which the component surface is coupled to the atmosphere. Multiple-source models (e.g., Norman et al. 1995) by definition deal with these components separately. Single-source models cannot; therefore, they require some type of adjustment to r_{ah}, which can only be done a priori on an empirical basis (Stewart et al. 1994). Kustas et al. (1989) and Kustas et al. (1994a) observed that in treating z_{oh} as a fitting parameter to attain good flux estimates over a sparse canopy with a single-source model, the value of z_{oh} expressed in dimensionless form as $\ln(z_{om}/z_{oh})$, required by Eq (1), was strongly correlated to $u(T_s - T_{air})$, where u is the wind speed. The value of z_{oh}, as seen in $T_s - T_{air}$ as an observational surrogate, would likely be a significant source of variability in r_{ah} across the site.

In summary then, the variabilities in z_{om} and z_{oh} (or any equivalent parameter that might serve the purpose of adjusting a single-source bulk transfer expression for what is actually a multisource surface) are likely to be the largest sources of variability in r_{ah} across the site. The determination of z_{oh} in any way other than a semi-empirical approach is not feasible. Future work for this study site will include the implementation of a relatively simple multiple-source model, such as that proposed by Norman et al. (1995) on a pixel-by-pixel basis.

Currently, there are no operational sensors from which spatially distributed information about z_{om} can be derived. Several different remotely sensed data types have the potential to yield information related to surface roughness (e.g., radar systems and laser altimeter systems), but research on the estimation of z_{om} from these data sources is just beginning. Menenti and Ritchie (1994) estimated local-scale values of z_{om} over the eight METFLUX stations involved in the Monsoon '90 experiment using laser altimeter data acquired along narrow aircraft transects. The results compared favorably with ground measurements. With this promising result as a basis, Kustas and Humes (1997) have begun to develop and test an algorithm for extending flux estimates from a flux station to other areas of a watershed by using remotely sensed surface temperatures and values of z_{om}. The approach to the estimation of roughness length is necessarily quite dependent on the spatial scale over which one is attempting to estimate surface fluxes. Our main focus here, and in the companion paper (Kustas and Humes 1997), is on the local roughness one would observe at length scales on the order of several hundred meters.

3) Mapping the sensible heat flux across the basin

The eventual goal in computing spatially distributed sensible heat flux maps is to utilize both spatially distributed values of z_{om} and surface temperature derived from remotely sensed data. However, the laser altimeter dataset used by Menenti and Ritchie (1994) only provides coverage over a very narrow transect line between METFLUX stations. Thus, due to limitations in the available datasets, it is not feasible at this time to apply the methods proposed by Menenti and Ritchie (1994) and Kustas and Humes (1997) to estimate r_{ah} values across the watershed on a pixel-by-pixel basis.

The more limited objective in this paper is to utilize the existing datasets to compute sensible heat flux maps that would best represent the instantaneous spatially distributed fluxes over the watershed. In light of that consideration and the fact that the r_{ah} values shown in Table 2 for the eight METFLUX stations indicated that typically there was not a high degree of variability in r_{ah} over the watershed during the times of the aircraft overpasses, it was decided that the most practical method for generating sensible heat flux maps with currently available data would be to use a spatially uniform value of r_{ah} over the watershed for each time period on the three days. The mean values of r_{ah} shown in Table 2 do not vary substantially from the median values for each of the 3 days, so the mean value of r_{ah} for each of the three days was used in Eq. (1) to compute the instantaneous sensible heat fluxes on a pixel-by-pixel basis.

In order to get an estimate of the uncertainty that might be inherent in estimating the sensible heat fluxes using the single uniform value for r_{ah}, the fluxes calculated with this procedure for the surface temperature extracts over each of the eight METFLUX sites on each of the three days are shown as the ordinate in Fig. 6. Plotted on the abscissa are the values of sensible heat flux measured with the ground-based flux stations. The solid line represents 1:1 agreement between the measured and computed fluxes. The root-mean-square error among the estimates for all eight stations on all three days is approximately 30 W m^{-2}, which is near the estimated uncer-

tainty in the ground measurements (Kustas et al. 1994b). It should be noted that this plot is not intended to be an independent validation of the procedure for calculating H, in that the average r_{ah} values used for the calculations were derived from the measured H values. Rather, it is intended to provide some estimate of how well the fluxes might be estimated by this procedure for other pixels in the watershed. Since the METFLUX stations do cover most of the extremes in vegetation differences across the watershed, as well as extremes in surface moisture and temperature differences, the variations between measured and computed fluxes for the eight METFLUX stations should be fairly representative of the expected variations between measured and computed fluxes for other pixels over the watershed.

The results of the pixel-by-pixel computation of the instantaneous spatially distributed sensible heat fluxes, using the spatially uniform values of r_{ah} for each day, are shown in Fig. 7. As would be expected because of the later time of data acquisition and the drier soil surface conditions, the values for DOY 213 are the highest for the 3 days (approximately 160–240 W m^{-2}). The dark areas in the map for DOY 213 correspond to surface areas obscured by clouds or cloud shadows on the original T_r image. As noted above, the discontinuity between the two flight lines, especially evident for DOY 213, arises from the difference in the time of data acquisition for the two flight lines, together with the very rapid rates of surface heating observed with clear sky conditions in a semiarid environment.

Between the acquisition of the image on DOY 213 and the image on DOY 216, both precipitation events shown in Fig. 4 (the event at 1444 on DOY 213 and the one at 2040 on DOY 215) and several other smaller events occurred. The precipitation contours for the smaller event that occurred on DOY 215 (approximately 10 h before the DOY 216 image data were acquired) are overlain on the sensible heat flux map for DOY 216 in Fig. 7. The areas of lowest sensible heat flux correspond to the areas that received the most precipitation in the event on the previous evening, although the eastern portions of the watershed also show significantly reduced H values, due to the moisture still available from the large event on DOY 213.

The cumulative precipitation contours from all the precipitation that occurred between DOYs 213 and 215 are overlain on the sensible heat flux map for DOY 221 in Fig. 7. Since the event on DOY 215 was much lighter than the one on DOY 213, the spatial effects of the DOY 215 event are not evident by DOY 221. Rather, the effects of the more major event on DOY 213 (and the smaller storms on DOY 214 that contributed additional precipitation to the far northeastern portion of the watershed) are controlling the pattern of surface drying and, thus, the sensible heat flux on DOY 221. The western portion of the watershed, which received less cumulative precipitation during the experimental period, shows consistently higher values of sensible heat flux. The persistence of the lower values of sensible heat flux in the northeastern portions of the watershed for more than five days after most of the precipitation occurred could be attributed to either one or both of the following mechanisms: 1) the availability of more moisture in the root zone of the vegetation in that portion of the watershed, making more moisture available for transpiration; and 2) the diurnal rewetting of surface soils typical in semiarid regimes (i.e., the delivery of moisture from lower in the profile to the surface in the nighttime and early morning hours), which would make more surface moisture available for bare soil evaporation. Gravimeteric measurements of near-surface layers 0–5 cm and 5–10 cm indicated that the moisture available in these layers was very much influenced by the depth of rainfall at each station and the time since precipitation. Time domain reflectometry measurements made at METFLUX sites 1 and 5 showed that the soil moisture available in the 15–30-cm layer, though somewhat lower at the western end of the watershed than at the eastern end, was relatively constant at each site throughout the experimental period (Kustas et al. 1993). The dominantly grass-type vegetation on the eastern edge of the watershed would be expected to have a greater capacity for moisture uptake from the relatively shallow depths (i.e., 0–15 cm) than would the dominantly shrub-type vegetation on the western edge of the watershed. Together, these observations suggest that at the eastern end of the watershed both the bare soil evaporation and the transpiration components of evapotranspiration were likely to be contributing to higher latent heat fluxes, and thus lower sensible heat fluxes, than those observed over the drier shrub-dominated areas in the western portion of the watershed.

4. Summary and future work

Spatially distributed radiometric surface temperatures over a semiarid watershed were computed using remotely sensed data acquired with an aircraft-based multispectral scanner during the Monsoon '90 Large Scale Field Experiment. The multispectral scanner data provided watershed coverage at a pixel resolution of 6.3 m and nearly daily temporal resolution. Surface temperature images acquired at midmorning on three particular days of the experiment were used for these analyses. At high spatial resolution, the surface temperature values appear to be correlated strongly with surface aspect; at more coarse spatial resolution, the surface temperatures variations across the watershed appear to be correlated with background soil moisture variations caused by highly localized precipitation events. The surface temperature data were aggregated to 400-m spatial resolution for the purpose of computing spatially distributed sensible heat fluxes over the watershed.

The eventual goal in computing spatially distributed sensible heat flux maps is to utilize both spatially distributed values of r_{ah} and surface temperature derived from remotely sensed data. However, due to limitations

in the datasets available at this time, the more limited objective in this paper was to utilize the existing datasets to compute sensible heat flux maps that would best represent the instantaneous spatially distributed fluxes over the watershed. By examination of the variability in r_{ah} over the site for the period of the overpass, it was determined that a spatially uniform value of r_{ah} derived from an average of the eight METFLUX stations would provide the most reliable maps of sensible heat flux. The maps of sensible heat flux computed with this procedure for the three different days indicated that the spatial patterns in sensible heat flux tracked well with the localized precipitation events that occurred over the watershed before and between the images acquired on three different days.

Future work will focus on more generalized techniques for the estimation of spatially distributed flux estimates, especially the evaluation of spatially distributed estimates of aerodynamic roughness length, which could be used to compute spatially variable transfer coefficients. The z_{om} values derived from laser altimeter data acquired over transects between the flux stations (Menenti and Ritchie 1994) can be extrapolated over the rest of the basin with the assistance of land use classifications derived from other remotely sensed data types. The methodology proposed by Kustas and Humes (1997) will then be applied on a pixel-by-pixel basis to generate improved spatially distributed maps of sensible heat flux utilizing spatially variable transfer coefficients. Additionally, a more physically based dual-source model (Norman et al. 1995) will be implemented on a pixel-by-pixel basis and the results compared to other approaches, including more complicated approaches such as those mentioned in the introductory section.

REFERENCES

Hall, F. G., K. F. Huemmrich, S. J. Goetz, P. J. Sellers, and J. E. Nickeson, 1992: Satellite remote sensing of surface energy balance: Success, failures and unresolved issues in FIFE. *J. Geophys. Res.*, 97(D17), 19061–19089.

Hipps, L. E., E. Swiatek, and W. P. Kustas, 1994: Interactions between regional surface fluxes and the ABL over a heterogeneous watershed. *Water Resour. Res.*, 30, 1387–1392.

——, K. S. Humes, and W. P. Kustas, 1995: An approach for quantifying the scales of inhomogeneity of surface properties, and the implications for simulating surface-atmosphere exchanges. *Proc. Conf. on Hydrology*, Dallas, TX, Amer. Meteor. Soc., 141–142.

Holwill, C. J., and J. B. Stewart, 1992: Spatial variability of evaporation over the FIFE area derived from aircraft and ground-based data. *J. Geophys. Res.*, 97(D17), 18673–18680.

Humes, K. S., W. P. Kustas, M. S. Moran, W. D. Nichols, and M. A. Weltz, 1994: Variability in emissivity and surface temperature over a sparsely vegetated surface. *Water Resour. Res.*, 30, 1299–1310.

——, ——, T. J. Schmugge, M. S. Moran, and L. E. Hipps, 1997: Radiometric surface temperature derived from NS001 multispectral scanner data. *Remote Sens. Environ.*, in press.

Jackson, R. D., 1985: Evaluating evapotranspiration at local and regional scales. *Proc. IEEE*, 73, 1086–1095.

Kniezys, F. X., E. P. Shettle, L. W. Abreu, J. H. Chetwynd, and G. P. Anderson, 1988: User guide to Lowtran 7. Air Force Geophysical Laboratory Rep. AFGL-TR-88-0177, 110 pp. [Available from Hanscom AFB, MA 01731.]

Kustas, W. P., and D. C. Goodrich, 1994: Preface to special issue on MONSOON '90 multidisciplinary experiment. *Water Resour. Res.*, 30, 1211–1225.

——, and K. S. Humes, 1997: Spatially distributed sensible heat flux over a semiarid watershed. Part II: Use of a varible resistance approach with radiometric surface temperatures. *J. Appl. Meteor.*, 36, 293–301.

——, B. J. Choudhury, M. S. Moran, R. J. Reginato, R. D. Jackson, L. W. Gay, and H. L. Weaver, 1989: Determination of sensible heat flux over sparse canopy using thermal infrared data. *Agric. For. Meteor.*, 44, 197–216.

——, and Coauthors, 1991: An interdisciplinary field study of the energy and water fluxes in the atmosphere-biosphere system over semiarid rangelands: Description and some preliminary results. *Bull. Amer. Meteor. Soc.*, 72, 1683–1705.

——, T. J. Schmugge, K. S. Humes, M. A. Weltz, T. J. Jackson, and R. Parry, 1993: Relationships between evaporative fraction and remotely sensed vegetation index and microwave brightness temperature for semiarid rangelands. *J. Appl. Meteor.*, 32, 1781–1790.

——, M. S. Moran, K. S. Humes, D. I. Stannard, P. J. Pinter Jr., L. E. Hipps, E. Swiatek, and D. C. Goodrich, 1994a: Surface energy balance estimates at local and regional scales using optical remote sensing from an aircraft platform and atmospheric data collected over semiarid rangelands. *Water Resour. Res.*, 30, 1241–1259.

——, J. H. Blanford, D. I. Stannard, C. S. T. Daughtry, W. D. Nichols, and M. A. Weltz, 1994b: Local energy flux estimates for unstable conditions using variance data in semiarid rangelands. *Water Resour. Res.*, 30, 1351–1361.

Menenti, M., and J. C. Ritchie, 1994: Estimation of effective aerodynamic roughness of Walnut Gulch watershed with laser altimeter measurements. *Water Resour. Res.*, 30, 1329–1337.

Moran, M. S., R. D. Jackson, L. H. Raymond, L. W. Gay, and P. N. Slater, 1990: Mapping surface energy balance components by combining Landsat Thematic Mapper and ground-based meteorological data. *Remote Sens. Environ.*, 30, 77–87.

——, W. P. Kustas, A. Vidal, D. I. Stannard, J. H. Blanford, and W. D. Nichols, 1994: Use of ground-based remotely sensed data for surface energy balance evaluation of a semiarid rangeland. *Water Resour. Res.*, 30, 1339–1349.

Norman, J. M., W. P. Kustas, and K. S. Humes, 1995: A two-source approach for estimating soil and vegetation fluxes from observations of directional radiometric surface temperature. *Agric. For. Meteor.*, 77, 263–293.

Reginato, R. J., R. D. Jackson, and P. J. Pinter Jr., 1985: Evaporation calculated from remote multispectral and ground station meteorological data. *Remote Sens. Environ.*, 18, 75–89.

Schmugge, T. J., T. J. Jackson, W. P. Kustas, R. Roberts, R. Parry, D. C. Goodrich, S. Amer, and M. Weltz, 1994: PBMR observations of surface soil moisture in MONSOON '90. *Water Resour. Res.*, 30, 1321–1327.

Sellers, P. J., Y. Mintz, Y. C. Sud, and A. Dalcher, 1986: A simple biosphere model (SiB) for use within general circulation models. *J. Atmos. Sci.*, 43, 505–531.

Stewart, J. B., W. P. Kustas, K. S. Humes, W. D. Nichols, M. S. Moran, and H. A. R. deBruin, 1994: Sensible heat flux-radiometric surface temperature relationship for eight semiarid areas. *J. Appl. Meteor.*, 33, 1110–1117.

Taconet, O., R. Berand, and D. Vidal-Madjar, 1986: Evapotranspiration over an agricultural region using a surface flux/temperature model based on NOAA-AVHRR data. *J. Climate Appl. Meteor.*, 25, 284–307.

Weltz, M. A., J. C. Ritchie, and H. D. Fox, 1994: Comparison of laser and field measurements of vegetation height and canopy cover. *Water Resour. Res.*, 30, 1311–1319.

Wukelic, G. E., D. E. Gibbons, L. M. Martucci, and H. P. Foote, 1989: Radiometric calibration of Landsat Thematic Mapper thermal band. *Remote Sens. Environ.*, 28, 339–347.